Coordinating carbon and nitrogen metabolic signaling through the cyanobacterial global repressor NdhR

Yong-Liang Jiang[a,b,c,1], Xue-Ping Wang[a,b,c,1], Hui Sun[a,b,c,1], Shu-Jing Han[a,b,c], Wei-Fang Li[a,b,c], Ning Cui[a,b,c], Gui-Ming Lin[d], Ju-Yuan Zhang[d], Wang Cheng[a,b,c], Dong-Dong Cao[a,b,c], Zhi-Yong Zhang[a,b,c], Cheng-Cai Zhang[d,2], Yuxing Chen[a,b,c,2], and Cong-Zhao Zhou[a,b,c,2]

[a]Hefei National Laboratory for Physical Sciences at the Microscale, University of Science and Technology of China, Hefei, Anhui, 230027, People's Republic of China; [b]School of Life Sciences, University of Science and Technology of China, Hefei, Anhui, 230027, People's Republic of China; [c]Key Laboratory of Structural Biology, Chinese Academy of Sciences, Hefei, Anhui, 230027, People's Republic of China; and [d]Key Laboratory of Algal Biology, Institute of Hydrobiology, Chinese Academy of Sciences, Wuhan, Hubei, 430072, People's Republic of China

Edited by Susan S. Golden, University of California, San Diego, La Jolla, CA, and approved December 8, 2017 (received for review September 14, 2017)

The coordination of carbon and nitrogen metabolism is essential for bacteria to adapt to nutritional variations in the environment, but the underlying mechanism remains poorly understood. In autotrophic cyanobacteria, high CO_2 levels favor the carboxylase activity of ribulose 1,5 bisphosphate carboxylase/oxygenase (RuBisCO) to produce 3-phosphoglycerate, whereas low CO_2 levels promote the oxygenase activity of RuBisCO, leading to 2-phosphoglycolate (2-PG) production. Thus, the 2-PG level is reversely correlated with that of 2-oxoglutarate (2-OG), which accumulates under a high carbon/nitrogen ratio and acts as a nitrogen-starvation signal. The LysR-type transcriptional repressor NAD(P)H dehydrogenase regulator (NdhR) controls the expression of genes related to carbon metabolism. Based on genetic and biochemical studies, we report here that 2-PG is an inducer of NdhR, while 2-OG is a corepressor, as found previously. Furthermore, structural analyses indicate that binding of 2-OG at the interface between the two regulatory domains (RD) allows the NdhR tetramer to adopt a repressor conformation, whereas 2-PG binding to an intradomain cleft of each RD triggers drastic conformational changes leading to the dissociation of NdhR from its target DNA. We further confirmed the effect of 2-PG or 2-OG levels on the transcription of the NdhR regulon. Together with previous findings, we propose that NdhR can sense 2-OG from the Krebs cycle and 2-PG from photorespiration, two key metabolites that function together as indicators of intracellular carbon/nitrogen status, thus representing a fine sensor for the coordination of carbon and nitrogen metabolism in cyanobacteria.

carbon metabolism | nitrogen metabolism | transcription factor | 2-oxoglutarate | 2-phosphoglycolate

Carbon and nitrogen are the two most abundant nutrient elements for living organisms. Therefore, the homeostasis of carbon and nitrogen metabolisms, which are fundamental to all forms of life to allow acclimation to fluctuating conditions, needs to be tightly controlled via diverse mechanisms. In autotrophic microorganisms such as cyanobacteria, the control of carbon metabolism is particularly important because of their limited choice of carbon sources to keep pace with nitrogen assimilation. Therefore, cyanobacteria constitute an ideal model for investigating the coordination of carbon and nitrogen metabolisms. Cyanobacteria are able to perform oxygen-evolving photosynthesis and use different forms of nitrogen sources such as nitrate, ammonium, and/or N_2 for diazotrophic strains (1). These nitrogen sources are converted into ammonium, which is then incorporated into the carbon skeleton 2-oxoglutarate (2-OG) for biosynthesis of various biomolecules (1). Thus, the accumulation of 2-OG in vivo constitutes the nitrogen-starvation signal and elicits a series of cellular responses, including the formation of nitrogen-fixing heterocysts in some filamentous cyanobacterial strains (2). The trimeric protein PII and the transcription factor NtcA constitute two well-established receptors of 2-OG in the nitrogen-starvation–signaling pathways in cyanobacteria (3). Each monomer of PII possesses a flexible T-loop protruding outwards to interact with the partner proteins (4). The binding of 2-OG and/or other effectors enables the T-loop to adopt various conformations to interact with diverse partners (5). NtcA is a transcription factor belonging to the cAMP receptor protein and fumarate/nitrate reductase regulator (Crp-Fnr) family, and the binding of 2-OG leads to a conformational change that enhances the DNA-binding ability of NtcA (6, 7).

As autotrophic organisms, cyanobacteria use inorganic carbon (Ci), including CO_2 and bicarbonate, as the major carbon source for growth. They are capable of acclimating and growing under a wide range of ambient CO_2 concentrations, thanks to the CO_2-concentrating mechanism (CCM). The CCM is the primary carbon-acquisition pathway for actively accumulating Ci into CO_2 fixation by ribulose-1,5-bisphosphate carboxylase/oxygenase (RuBisCO) within microcompartments termed "carboxysomes" (8). To guarantee the high efficiency of the Calvin–Benson cycle, the cyanobacterial CCM could functionally compensate for the poor affinity and selectivity of RuBisCO toward CO_2 (9, 10). The CCM requires a number of genes involved in bicarbonate transport, CO_2 uptake, and other related energetic or regulatory processes and thus its activities are highly coordinated (8, 11). In *Synechocystis* sp. PCC 6803 (hereafter "*Synechocystis*"), the CCM is mainly under the

Significance

The homeostasis of carbon and nitrogen metabolism needs to be tightly regulated for cell acclimation to fluctuating environments. The related metabolic pathways are ultimately coordinated by the master transcription factors that sense the intracellular metabolites. We report here biochemical, structural, and functional studies of the fine regulation of the transcriptional repressor NAD(P)H dehydrogenase regulator (NdhR). Two key metabolites, 2-OG from the Krebs cycle and 2-PG from photorespiration, have opposite effects on the regulatory activity of NdhR. We propose that 2-OG and 2-PG function together as indicators of intracellular carbon/nitrogen status and that NdhR senses these two effectors in a mutually exclusive manner. Our findings together with previous studies provide a model for the fine coordination of carbon and nitrogen metabolic signaling.

Author contributions: Y.-L.J., C.-C.Z., Y.C., and C.-Z.Z. designed research; Y.-L.J., X.-P.W., H.S., S.-J.H., N.C., G.-M.L., J.-Y.Z., D.-D.C., and Z.-Y.Z. performed research; Y.-L.J., X.-P.W., H.S., W.-F.L., W.C., C.-C.Z., Y.C., and C.-Z.Z. analyzed data; and Y.-L.J., C.-C.Z., and C.-Z.Z. wrote the paper.

The authors declare no conflict of interest.

This article is a PNAS Direct Submission.

Data deposition: The atomic coordinates and structure factors have been deposited in the Protein Data Bank, www.wwpdb.org (PDB ID codes 5Y2V for the full-length NdhR complexed with 2-OG and 5Y2W for the NdhR RD domain complexed with 2-PG).

[1]Y.-L.J., X.-P.W., and H.S. contributed equally to this work.

[2]To whom correspondence may be addressed. Email: zcz@ustc.edu.cn, cczhang@ihb.ac.cn, or cyxing@ustc.edu.cn.

This article contains supporting information online at www.pnas.org/lookup/suppl/doi:10.1073/pnas.1716062115/-/DCSupplemental.

control of two LysR-type transcriptional regulators (LTTRs), namely NAD(P)H dehydrogenase regulator (NdhR)/Sll1594 (also known as "CcmR") (12–15) and CmpR/Sll0030 (16, 17). CmpR functions as a transcriptional activator to up-regulate the expression of the Ci-responsive *cmp* operon that encodes the HCO_3^- transporter CmpABCD under Ci-limiting conditions (16). In contrast, despite sharing a sequence identity of 54% with CmpR, NdhR acts as a repressor to globally control the expression of several CCM-related genes, including the gene clusters containing *ndhF3/ndhD3/cupA/sll1735* (the *ndh-I3* operon), which encode the high-affinity CO_2-uptake system proteins, the *sbtA/B* genes encoding the Na^+/HCO_3^- symporter, the *mnh* operon, and *bicA* (13). Moreover, similar to most LTTR proteins, NdhR also negatively autoregulates the expression of its own gene *ndhR* (12). The promoter region recognized by NdhR usually consists of two tandem repetitive motifs with a consensus sequence of ATAG-N_8-CTAT that overlap the transcription start site (18). A previous report found that in *Synechocystis*, $NADP^+$ and the metabolic intermediate 2-OG enhance the binding of NdhR to its own promoter as well as to the promoter region of the *ndh-I3* operon and thereby appear to act as corepressors (19). In addition, binding of CmpR to the *cmp* operon could be significantly elevated in the presence of ribulose-1,5-bisphosphate (RuBP) or 2-phosphoglycolate (2-PG) in *Synechococcus* (17). However, no direct evidence is available to support the effector function of these metabolites, and the binding pattern and regulatory mechanism remain unknown.

RuBisCO is a bifunctional enzyme that can use either CO_2 (carboxylase) or O_2 (oxygenase) as the substrate (20). Under high CO_2 (HC) levels, it acts as a carboxylase to convert CO_2 into 3-phosphoglycerate to feed the Calvin–Benson cycle, thus providing carbon sources for cell growth. When the CO_2 levels become limiting, the oxygenase activity is favored, which leads to the synthesis of both 3-phosphoglycerate and 2-PG, which is then metabolized in the photorespiratory cycle (21). During the primary response, a carbon limitation in the cells can also be considered as a nitrogen oversupply which will drain the carbon skeleton 2-OG for nitrogen assimilation through the glutamine synthetase–glutamate synthase pathway (3), thus most likely leading to a lower level of 2-OG. Therefore, the level of 2-PG is somewhat inversely related to that of 2-OG, and vice versa. These findings raise a number of questions. How do cyanobacteria sense the intracellular carbon status? Does 2-OG alone suffice to reflect the nitrogen metabolic status as well as the N/C balance? Are other receptors of the 2-OG signal, in addition to NtcA and PII, involved in the control of nitrogen or carbon metabolism? To answer these questions, we characterized NdhR, a transcriptional repressor involved in the control of carbon metabolism, including that of the CCM in cyanobacteria. We solved the full-length structure of NdhR from *Synechocystis* in complex with 2-OG as well as the complex structure of the NdhR regulatory domain with 2-PG. Further biochemical and genetic experiments suggested that the metabolites 2-PG and 2-OG act as an inducer and a corepressor, respectively, to cooperatively regulate CCM via NdhR. Our findings provide structural insights into the regulatory mechanism of LTTR repressors and reveal a connection between the carbon and nitrogen metabolisms.

Results

2-OG and 2-PG Are the Effectors of NdhR. The transcriptional activity of an LTTR is usually modulated upon binding of small molecule(s) (22). NdhR is a repressor that regulates genes or gene clusters involved in the CCM (13), in which several metabolites, such as 2-PG, 2-OG, RuBP, and $NADP^+$, have been suggested to act as internal signals for the deprivation of inorganic carbon (8, 17, 23). Of note, RuBP and 2-PG were found to enhance the binding of CmpR to the promoter region of the *cmp* operon (17) but did not affect the DNA-binding activity of NdhR (19). By contrast, 2-OG and $NADP^+$ were reported to enhance the binding of NdhR to its own gene promoter as well as to that of *ndh-I3* and thereby seemed to be corepressors (19). To identify the effectors of NdhR, we applied surface plasmon resonance (SPR) assays by immobilizing the NdhR proteins on the chip to detect the binding affinity of NdhR toward the potential metabolites 2-PG, 2-OG, RuBP, and $NADP^+$. The results showed that 2-OG and 2-PG, but not RuBP and $NADP^+$, could bind to NdhR (Fig. 1*A*). Further experiments enabled us to calculate the dissociation constants (K_ds) at 0.55 mM for 2-OG (Fig. 1*B*) and at 0.43 mM for 2-PG (Fig. 1*C*), which are comparable to the intracellular concentrations of these metabolites under physiological conditions (24). Notably, the binding affinity of NdhR toward 2-OG is comparable to that of previously reported interactions between repressors and corepressors, such as *Escherichia coli* MetJ and Trp (25, 26). These results strongly indicated that 2-OG and 2-PG are effectors of NdhR.

To further investigate if 2-OG and 2-PG indeed alter the DNA-binding affinity of NdhR, we applied the SPR assays with DNA immobilized on the chip to determine the binding affinity of NdhR toward the 140-bp *ndhR* promoter sequence (18). NdhR displays a strong binding affinity toward the target DNA, at a K_d of 45 nM (Fig. 1*D*). The DNA-binding affinity of NdhR is increased to a K_d of 27 nM upon the addition of 2-OG (Fig. 1*E*), which is in accordance with the previous results (19). By contrast, the addition of 2-PG sharply reduced the DNA-binding affinity of NdhR, resulting in a K_d of 5,210 nM (Fig. 1*F*). These results suggested that 2-PG significantly alleviates the interaction of NdhR with the *ndhR* promoter region, whereas 2-OG has the opposite effect. Thus, 2-PG acts as an inducer of NdhR, and the effect of 2-OG is consistent with its corepressor function, as previous suggested (19).

Crystal Structure of NdhR. To provide evidence of the effector function of 2-OG and 2-PG and to gain insight into the regulatory mechanism of NdhR, we solved the crystal structure of the full-length NdhR at 2.60 Å. Each asymmetric unit contains four subunits assembling into a tetramer (Fig. 2*A*). Similar to typical LTTRs, the NdhR tetramer consists of two compact subunits and two extended subunits (Fig. 2*B*). Each subunit is composed of a DNA-binding domain (DBD) and a regulatory domain (RD) connected by a short hinge region (Fig. 2*C*). The DBD consists of four α-helices (α1–α4) flanked by two β-strands (β1–β2) (Fig. 2*B*), with a winged helix-turn-helix (wHTH) DNA-binding region (27, 28). The RD could be further divided into two subdomains, RD1 and RD2, both of which adopt an α/β Rossman-like fold and are connected to each other with two crossover β-strands,

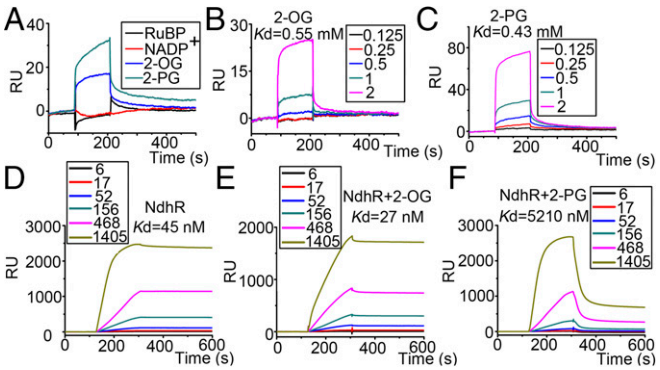

Fig. 1. Binding affinity assays of NdhR toward small molecules or target DNA. (*A*) The SPR difference curves of NdhR in the presence of different molecules at a final concentration of 1 mM. The NdhR proteins were immobilized on the surface of the CM5 chip to test the binding of different ligands. RU, response units. One RU represents the binding of 1 pg of protein per square mm. (*B* and *C*) The binding of NdhR with 2-OG (*B*) and 2-PG (*C*) ranging from 0.125–2 mM. K_d values are shown. (*D–F*)The DNA-binding affinity of NdhR alone (*D*) and NdhR in the presence of 2-OG (*E*) or 2-PG (*F*). The 140-bp DNA was derived from the promoter region of the *ndhR* gene and then was immobilized on the chip. NdhR was diluted at a series of concentrations from 6–1,405 nM. 2-OG or 2-PG was added at a final concentration of 5 mM.

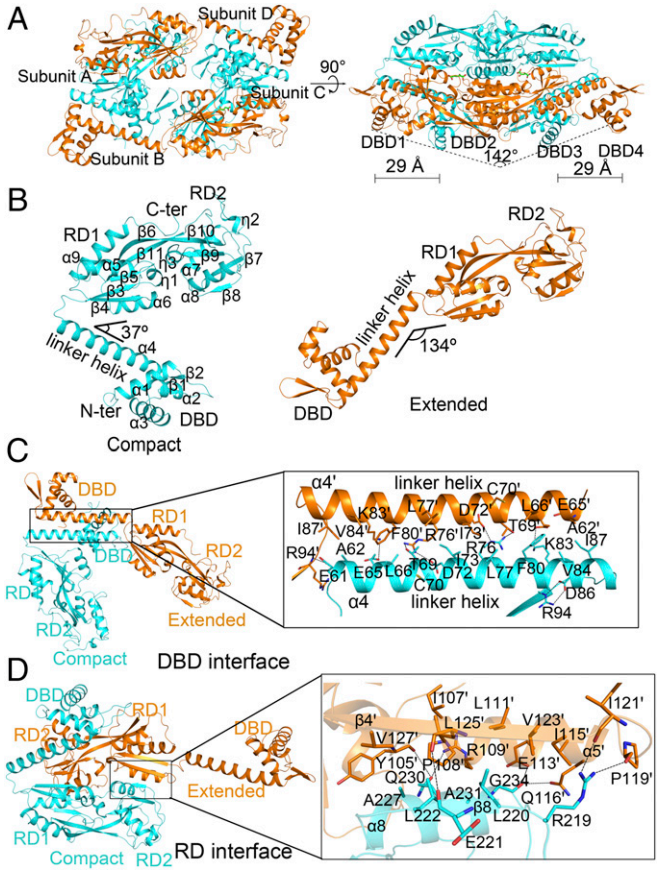

Fig. 2. The tetrameric structure of NdhR. (*A*) The tetrameric structure of NdhR, shown in two different views. Each tetramer is composed of two compact subunits (in cyan) and two extended subunits (in orange). (*B*) Cartoon presentation of the compact and extended subunits of NdhR, with the secondary structural elements labeled sequentially. (*C* and *D*) DBD-mediated (*C*) and RD-mediated (*D*) interfaces of NdhR. (*Insets*) The detailed interaction networks. The interacting residues are shown as sticks, and the polar interactions are indicated by dashed lines.

β6 and β11 (Fig. 2*B*). RD1 and RD2 pack against each other to form a cleft 10 Å in depth and 20 Å in width.

The two compact subunits are quite similar to each other, with an rmsd of 0.44 Å over 266 Cα atoms, whereas the two similar extended subunits share an rmsd of 0.31 Å over 289 Cα atoms. In the compact subunit, the DBD and RD are close to each other, with an interdomain angle of ∼37° (Fig. 2*B*). Of note, Asp86 from the DBD forms two salt bridges with Arg94 from RD1. However, in the extended subunit, the DBD and RD stay away from each other, with an interdomain angle of 134° (Fig. 2*B*). Nevertheless, either the individual DBDs or RDs are almost the same in the compact and extended subunits, which differ from each other due to rigid-body rotation.

In the tetrameric assembly, four DBDs of NdhR project outward and form a V-shaped surface along the DNA-binding helices of the tetramer, with an angle of ∼142° (Fig. 2*A*). This arrangement of DBDs indicated that the NdhR tetramer most likely binds to and bends the target DNA. The tetrameric assembly of NdhR can be regarded as a dimer of dimers in which each dimer comprises one compact and one extended subunit. The helices α4 and α4′ from two DBDs form an antiparallel coiled-coil that contributes to the majority of dimeric interface (Fig. 2*C*). In detail, the ∼1,700-Å^2 dimeric interface is stabilized mainly by hydrophobic interactions in addition to several hydrogen bonds (Fig. 2*C*). This type of DBD-mediated dimer is highly conserved among all LTTRs of known structure (28–35). The dimer could be further assembled into a tetramer via the interactions between two RDs (Fig. 2*D*). The two RDs contact each other in an antiparallel, side-by-side alignment, forming an interface of 1,900 Å^2. α8 and β8 from RD2 of one subunit interact with β4′ and α5′ from RD1 of the symmetric subunit, and vice versa (Fig. 2*D*).

Typical LTTRs usually have a conserved structure with an N-terminal DBD and a C-terminal RD (36). To date, the crystal structures of LTTRs revealed a tetramer composed of two compact and two extended subunits (28–35), except for CrgA, which forms an octamer comprising only compact subunits (30). Despite sharing a tetramer structure, NdhR differs from other LTTRs in the relative positions and rotations of the DBDs against the RDs, in addition to the lengths of the linker helix. Another difference can be found at the variations of the RD domains in NdhR, especially the effector-binding cleft, suggesting that NdhR senses molecules that are different from those sensed by other LTTRs of known structure.

2-OG Binds at the Interface Between Two RDs and Acts as a Corepressor of NdhR. In the full-length structure of NdhR, two pieces of electron density were found at the interfaces between the RD domains. However, none of the molecules from the purification and crystallization buffers could fit the density. Instead, the density fits well with a molecule of 2-OG (Fig. 2*A*), an effector of NdhR according to our biochemical data and a previous report (Fig. 1*B*) (19). 2-OG is most likely incorporated during the heterogeneous expression of NdhR in *E. coli*, which possess an intracellular 2-OG concentration in the millimolar range (37). 2-OG binds to the residues Ser224, Asn225, Tyr105, and Lys104 from one RD and to the counterpart residues from the symmetric RD (Fig. 3*A*). Under conditions of carbon oversupply or nitrogen starvation, the intracellular concentration of 2-OG increases in cyanobacteria (38, 39); such conditions should favor the binding of 2-OG to the NdhR tetramer. The 2-OG–complexed NdhR adopts a conformation complementary to the DNA major groove, in agreement with the distance of 29 Å between the two recognition helices binding to the DNA palindrome (Fig. 3*A*) and therefore leading to repression of the NdhR regulon.

To confirm the repressor function of NdhR and the effect of 2-OG, we first constructed an *ndhR*-deletion strain. We found that the expression levels of NdhR-regulated genes, such as *ndhF3*, *sbtA*, and *bicA*, are significantly up-regulated (Fig. 3*B*), in agreement with a previous report (13). Afterwards, to check the in vivo effect of 2-OG on the activity of NdhR, we increased the intracellular 2-OG level by adding to the medium 20 mM dimethyl-ketoglutarate (dmKG), a membrane-permeable ester that is cleaved by intracellular esterase to produce 2-OG (40). Upon the increase of the intracellular 2-OG concentration, the expression levels of *ndhR*, *ndhF3*, *sbtA*, and *bicA* were significantly down-regulated compared with the control (Fig. 3*C*). Together, these findings demonstrate that 2-OG is an intrinsic corepressor that keeps NdhR bound to the target DNA to repress gene expression.

2-PG Binds at the Cleft of RDs of NdhR and Induces Gene Expression. The in vitro binding experiments indicated that 2-PG dramatically weakens the DNA-binding capability of NdhR toward its DNA targets (Fig. 1*F*). To elucidate the mechanism of 2-PG interaction with NdhR, we initially attempted to solve the full-length structure of NdhR in complex with 2-PG, but we failed to do so after extensive trials. Alternatively, we solved the structure of the RD domain of NdhR in complex with 2-PG at 2.20 Å. In each RD subunit, 2-PG binds to the cleft between RD1 and RD2 (Fig. 4*A*). The oxygen atoms of the phosphate group of 2-PG form hydrogen bonds with the side chains of Arg195, His130, Thr201, and Thr101. The carboxyl group of 2-PG is hydrogen-bonded with Thr102, Asn164, and Arg267 (Fig. 4*A*). Sequence alignment revealed that all these 2-PG–binding residues are highly conserved among NdhR and homologs. Compared with the structure of NdhR complexed with 2-OG, binding of 2-PG triggers a significant induced fit of the intradomain cleft between RD1 and RD2. In detail, upon 2-PG binding, the residues Asn164 from β6 and Arg267 from β11 at the bottom of the binding cleft

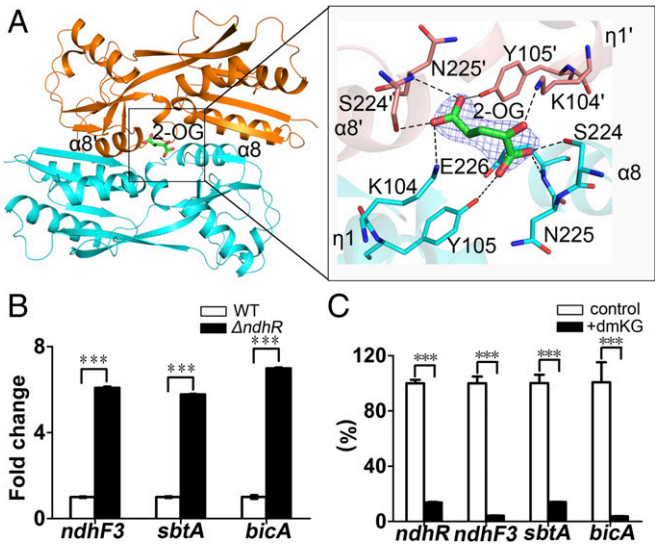

Fig. 3. 2-OG is a corepressor of NdhR. (*A*) The binding site of 2-OG. One 2-OG molecule binds at the interface between two RD domains. (*Inset*) The 2-OG molecule and the interacting residues are shown as sticks, and the polar interactions are marked by dashed lines. The 2Fo- Fc electron density map of 2-OG is shown as a blue mesh, countered at 1.5 σ. (*B*) The transcript abundance of NdhR-regulated genes in the wild-type strain (white bars) or *ndhR*-deletion strain (Δ*ndhR*, black bars). The cells were grown at ambient air conditions. (*C*) The transcript abundance of the NdhR-regulated genes without (control, white bars) or with the addition of dimethyl-ketoglutarate (dmKG, black bars). Data are presented as the means ± SD from three independent assays. A two-tailed Student's *t* test was used for the comparison of statistical significance; ***$P < 0.001$.

form hydrogen bonds with 2-PG, thus disrupting the previous β6 and β11 that cross over RD1 and RD2 (Fig. 4*B*). In consequence, RD1 and RD2 undergo a rigid-body rotation toward 2-PG, resulting in a rather compact conformation of the RD. With the two RD1 subdomains superimposed, RD2 rotates about ∼25° toward the cleft upon 2-PG binding (Fig. 4*B*). The conformational changes at the RD domains upon 2-PG binding further trigger the conformational changes in the overall structure of the NdhR tetramer, resulting in the altered DNA-binding capability of NdhR, as confirmed by the SPR assays. Notably, binding of 2-OG will stabilize the interface between the two RDs, thus excluding the binding of 2-PG to the intradomain cleft between RD1 and RD2, whereas the induced fit upon binding to 2-PG will disrupt the 2-OG–binding site (Fig. 4*B*). Thus, the binding of 2-PG or 2-OG to NdhR should be mutually exclusive.

To further examine the possible roles of 2-PG in NdhR's transcriptional regulation of its target genes, we constructed a recombinant strain overexpressing *slr0458*, which encodes a phosphoglycolate phosphatase (PGPase) [hereafter, the "PGPase-overexpression" (POE) strain]. This PGPase was reported to be responsible for the catabolism of intracellular 2-PG, which usually accumulates in the cell at a high level after 30 min after the shift from an HC to a limiting CO_2 level (LC) (23). qPCR analyses showed that the transcription level of the *slr0458* gene increased by ∼25-fold in the POE strain compared with the wild type (Fig. 4*C*). In the POE strain, due to the high level of PGPase that degrades the intracellular 2-PG, the transcription of NdhR target genes *ndhR*, *ndhF3*, *sbtA*, and *bicA* is significantly down-regulated, to about 20–60% of that in the wild-type strain (Fig. 4*D*), in agreement with the previous report on *ndhF3* and *sbtA* genes (23). To validate that the effect of 2-PG is mediated by NdhR in vivo, we also overexpressed *slr0458* in the *ndhR*-deletion strain. Although the transcription of *slr0458* is also up-regulated by ∼35-fold (Fig. 4*E*), the expression levels of NdhR target genes are comparable to those without the overexpression of *slr0458* (Fig. 4*F*). Taken together, these results further confirmed that 2-PG is an inducer that directly interacts with NdhR in vivo.

Discussion

LTTRs are the most ubiquitous transcriptional factors in prokaryotes, regulating various biological processes such as the fixation of CO_2 and N_2, cell division, oxidative response, and the synthesis or degradation of amino acids (41). They can act as either activators or repressors in transcriptional regulation. So far, the structures of only a few activator-type LTTRs have been reported, and a sliding dimer model was proposed to explain how effectors activate LTTRs (28–35). The recent structures of the ligand-binding domain of CysB from *Salmonella typhimurium* reveal two distinct binding sites that are allosterically coupled by two inducers (42). The overall structures of the RDs of NdhR and CysB are similar, with an rmsd of 2.90 Å over 167 Cα atoms, although CysB has two additional C-terminal helices and an unstructured tail. Moreover, the two proteins display distinct features in their ligand-binding mode. To the best of our knowledge, NdhR has only one inducer, namely 2-PG, binding to the intradomain cleft of RD, which corresponds to the primary binding site of CysB. In addition, the corepressor 2-OG of NdhR binds to the interface between the two RDs, which is different from the 2-PG–binding site. The present structural and biochemical analyses enabled us to propose a model for the regulation mechanism of the LTTR repressor NdhR, which is distinct from the allosteric coupling mechanism of CysB activation or that of other LTTR activators.

In the present study, we found that 2-OG and 2-PG, not RuBP or $NADP^+$, are effector molecules of NdhR. These two effectors display similar affinity toward NdhR but bind to different sites of the protein in a mutually exclusive manner. Structural analyses and biochemical characterizations combined with genetic studies indicate that the interactions between the two effectors and NdhR provoke different conformational changes, hence leading to opposite effects on the transcriptional activity of NdhR. As the

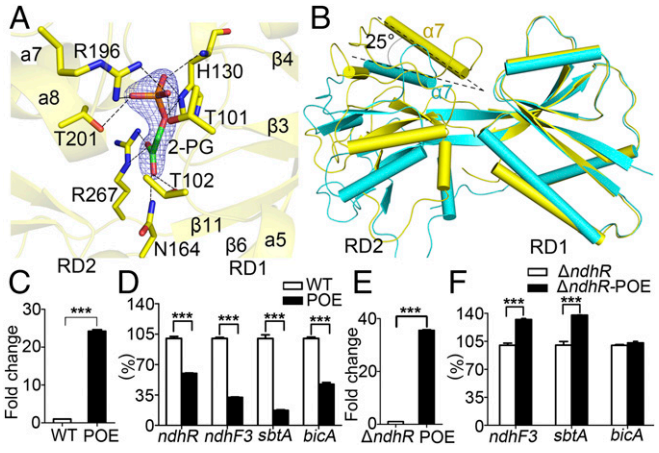

Fig. 4. 2-PG is an inducer of NdhR. (*A*) The binding site of 2-PG. The 2-PG molecule and the interacting residues are shown as sticks, and the polar interactions are marked by dashed lines. The 2Fo-Fc electron density map of 2-PG is shown as a blue mesh, countered at 1.5 σ. (*B*) Comparison of the RD domains in the presence of 2-PG (yellow) or 2-OG (cyan) with RD1 superimposed. (*C*) Comparison of the transcript abundance of *slr0458* in the wild-type (white bar) and POE (black bar) strains. For all in vivo experiments, total mRNA was extracted 30 min after the shift from the HC to the LC condition, and qPCR assays were used to assess the relative level of relevant genes. The cells were cultured in ambient air for the LC condition and in ambient air supplemented with 5% (vol/vol) CO_2 for the HC condition. (*D*) Transcript abundance of NdhR-regulated genes in the wild-type (white bars) and POE (black bars) strains. (*E*) Comparison of the transcript abundance of *slr0458* in the *ndhR*-deletion strain without Slr0458 (Δ*ndhR*, white bar) or with overexpressed Slr0458 (Δ*ndhR*-POE, black bar). (*F*) Transcript abundance of NdhR-regulated genes in the *ndhR*-deletion strain without (Δ*ndhR*, white bars) or with (Δ*ndhR*-POE, black bars) overexpressed Slr0458. Mean values represent at least three independent experiments. A two-tailed Student's *t* test was used for the comparison of statistical significance; ***$P < 0.001$.

levels of 2-PG and 2-OG are reversely correlated, their relative changes synergistically coordinate the NdhR-regulated transcription (Fig. 5*A*). Our present data together with previous findings (3, 8, 12, 13, 23) enable us to propose a detailed model of the molecular mechanism allowing cyanobacteria to adapt to relative changes in the status of carbon and nitrogen metabolism mediated by NdhR (Fig. 5*A*). Noticeably, the coordination of carbon and nitrogen balance is achieved through a network of regulators, such as PII, NtcA (7, 43), and the phosphotransferase system (44). Moreover, the cyanobacterial CCM is regulated by a transcriptional network of NdhR, CmpR, and an AbrB family member, Sll0822 (45) for acclimation to fluctuating environments (8). The model presented here is simplified for clarity and emphasizes only the role of NdhR in coordinating carbon and nitrogen balance. Nevertheless, our model provides structural insights into the regulation of NdhR allowing the coordinated response of part of the high-affinity Ci-uptake system and also expands previous findings on the regulation of CCM by NdhR and CmpR (19).

The cyanobacterial CCM elevates the CO_2 concentration near RuBisCO to enhance CO_2 fixation in the carboxysome, which is the primary carbon source for the Calvin–Benson cycle in photosynthesis (8). When environmental Ci is sufficient, the higher CO_2/O_2 ratio around the catalytic site of RuBisCO activates its carboxylation activity, which assimilates CO_2 to produce 3-phosphoglycerate (46); meanwhile, the oxygenase function of Rubisco is inactive, leading to a low concentration of 2-PG in the cell (Fig. 5*B*). The newly fixed organic triose can feed the Krebs cycle (Fig. 5*B*), in which the 2-OG dehydrogenase is replaced by two alternative enzymes, 2-OG decarboxylase and succinic semialdehyde dehydrogenase, to convert the intermediate 2-OG to succinate (39). In addition, 2-OG is also a primary carbon skeleton for the assimilation of ammonia that bridges the Krebs cycle and the glutamate/glutamine metabolism shunt (Fig. 5*B*). The central metabolite 2-OG has been shown to be a signal of nitrogen starvation, and its binding to PII and NtcA enables the cells to respond to nitrogen deficiency (3). Thus, when the 2-PG level is low due to high CO_2 input in the cells, the relative level of 2-OG increases to augment nitrogen assimilation through NtcA and PII (7, 43); at the same time, the NdhR tetramer binds to two molecules of the corepressor 2-OG at the interface between two adjacent RDs (Fig. 5*A*). Due to its high affinity for two tandem consensus motifs, ATAG-N_8-CTAT, at the core promoter region around −10 sites (18), the 2-OG–complexed NdhR is a strong repressor that blocks the binding site of RNA polymerase, causing a decrease in the transcription of CCM-related genes. Thus, increased nitrogen assimilation and decreased carbon input enable the cells to rebalance the carbon and nitrogen metabolism. On the contrary, when CO_2 input is low, the 2-PG concentration in the cells increases because of the oxygenase activity of RuBisCO; this will also lead to a lower level of 2-OG because of reduced carbon input into the Krebs cycle through the Calvin–Benson cycle. In such situations, four molecules of 2-PG bind to a NdhR tetramer at the intradomain cleft of the RD, which triggers a significant induced fit that alters the interface between the two adjacent RDs, thus excluding the binding of 2-OG. Moreover, molecular dynamics simulations indicated that, upon 2-PG binding, the RD domains undergo drastic conformational changes and trigger the rearrangements of the DBDs (Fig. S1). In the 2-OG–bound state, the distance between the DNA-recognition helices of adjacent DBDs is 29 Å, which matches a continuous DNA major groove, thus providing a stronger DNA binding and repression effect. By contrast, upon binding to 2-PG, the corresponding distance between DBDs is shifted to 25 Å, which is hard to fit into the DNA major groove. Accordingly, the DNA-binding affinity is sharply decreased, as shown by the SPR assays (Fig. 1*F*). In consequence, dissociation of NdhR enables the binding of RNA polymerase to the promoter region of NdhR-suppressed target genes (Fig. 5*A*). Thus, a high 2-PG level relieves the repressor effect of NdhR, allowing the transcription of genes related to CCM to increase carbon input, while the native forms of NtcA and PII lower nitrogen assimilation, so that carbon and nitrogen metabolisms are kept in balance. Additionally, the accumulation of 2-PG is also sensed by the activator CmpR (17), which in turn initiates the transcription of the *cmp* operon and thus further accelerates the carbon uptake rate. Considering the 54% sequence identity with NdhR, we speculate that CmpR binds to 2-PG in a pattern similar to 2-PG binding by NdhR, although CmpR and NdhR regulate gene expression in an opposite manner. Furthermore, our result strengthens the previous finding of the role of 2-PG as an internal signal of Ci deprivation (23). Sensing of the intracellular 2-PG level by both NdhR and CmpR suggests a positive feedback circuit for a rapid response to Ci deprivation. Overall, our findings together with the previous result regarding the role of 2-OG (19) further provide a structural basis explaining the coordination of global carbon and nitrogen assimilation during changes in Ci availability (13, 47, 48).

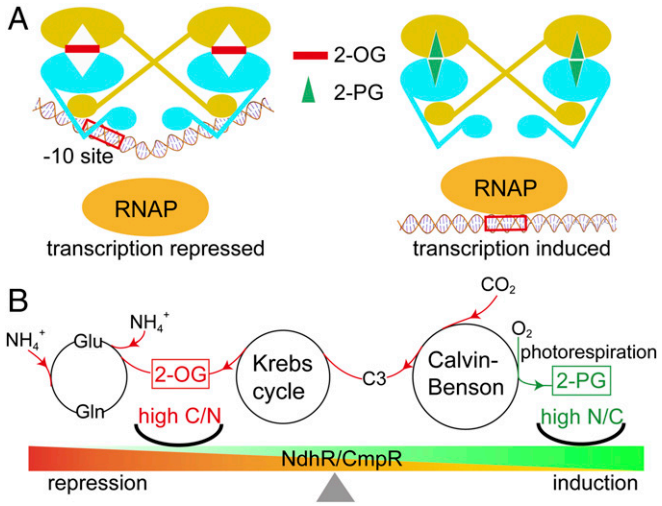

Fig. 5. NdhR-coordinated balance of carbon and nitrogen metabolisms. (*A*) A putative transcriptional regulation mechanism of NdhR. Upon the binding of 2-OG (red rectangle) at the RD interface, the NdhR tetramer (cyan for the compact subunits and orange for the extended subunits) binds to the flanking region of the −10 site (red box) through DBDs, leading to repressed transcription. Upon binding of 2-PG (green triangle) at the intradomain cleft of the RD, the NdhR tetramer undergoes drastic conformational changes and dissociates from the target DNA, enabling the recruitment of RNA polymerase (RNAP) to the −10 site and induction of transcription. (*B*) Coordinated carbon and nitrogen metabolisms via repression and induction of NdhR/CmpR. At the high-Ci condition, the newly fixed organic triose produced in the Calvin–Benson cycle feeds the Krebs cycle to create the pentose 2-OG, which links the glutamate/glutamine metabolism shunt. At the low-Ci condition, the predominant reaction of RuBisCO shifts from carboxylation to oxygenation of RuBP, leading to the production of 2-PG. 2-OG is an indicator of high C/N and keeps NdhR in the repressive state, whereas 2-PG indicates a high N/C level and triggers the induction/activation of NdhR/CmpR.

In summary, a balanced supply of carbon and nitrogen is necessary for the optimal growth of cells under varying environmental conditions. The accumulation of intracellular 2-OG is an indicator of a high C/N ratio (3), whereas the accumulation of the photorespiratory metabolite 2-PG is an indicator of a high N/C ratio (Fig. 5*B*). Imbalanced C/N metabolism will result in the intracellular accumulation of either 2-OG or 2-PG, and their interaction with global sensors, such as NtcA, CmpR, and NdhR, switches on or off the downstream genes involved in carbon and nitrogen metabolism and eventually leads to the restoration of balance. The opposite effects of 2-OG and 2-PG on the activity of NdhR provide an example of the integration of the metabolic signaling necessary for cyanobacterial adaptation in response to the cellular status of carbon or nitrogen metabolism.

Materials and Methods

The *ndhR* gene was cloned into the pET28a-derived vector and then was expressed in the *E. coli* BL21 strain. The proteins were purified by nickel-affinity

purification followed by size-exclusion chromatography. The structure of NdhR was solved by the single-wavelength anomalous dispersion phasing method. The *ndhR*-deletion strain was constructed by replacing the *ndhR* gene with the spectinomycin resistance gene via homologous recombination. The real-time qPCR experiments were carried out according to the protocols provided (Roche). For full details of all these processes, see *Supporting Information*.

ACKNOWLEDGMENTS. We thank the staff at the Shanghai Synchrotron Radiation Facility for technical assistance. This work is supported by National Natural Science Foundation of China (www.nsfc.gov.cn) Grants 31630001, 31500598, and 21573205, Strategic Priority Research Program of the Chinese Academy of Sciences Grant XDB08020300, Key Research Program of Frontier Sciences of the Chinese Academy of Sciences Grant QYZDJ-SSW-SMC016, and the Innovation Center for Cell Signaling Network.

1. Flores E, Herrero A (2005) Nitrogen assimilation and nitrogen control in cyanobacteria. *Biochem Soc Trans* 33:164–167.
2. Laurent S, et al. (2005) Nonmetabolizable analogue of 2-oxoglutarate elicits heterocyst differentiation under repressive conditions in *Anabaena* sp. PCC 7120. *Proc Natl Acad Sci USA* 102:9907–9912.
3. Huergo LF, Dixon R (2015) The emergence of 2-oxoglutarate as a master regulator metabolite. *Microbiol Mol Biol Rev* 79:419–435.
4. Xu Y, et al. (2003) The structures of the PII proteins from the cyanobacteria *Synechococcus* sp. PCC 7942 and *Synechocystis* sp. PCC 6803. *Acta Crystallogr D Biol Crystallogr* 59:2183–2190.
5. Forchhammer K (2008) P(II) signal transducers: Novel functional and structural insights. *Trends Microbiol* 16:65–72.
6. Zhao MX, et al. (2010) Structural basis for the allosteric control of the global transcription factor NtcA by the nitrogen starvation signal 2-oxoglutarate. *Proc Natl Acad Sci USA* 107:12487–12492.
7. Llácer JL, et al. (2010) Structural basis for the regulation of NtcA-dependent transcription by proteins PipX and PII. *Proc Natl Acad Sci USA* 107:15397–15402.
8. Burnap RL, Hagemann M, Kaplan A (2015) Regulation of CO_2 concentrating mechanism in cyanobacteria. *Life (Basel)* 5:348–371.
9. Price GD, Sultemeyer D, Klughammer B, Ludwig M, Badger MR (1998) The functioning of the CO_2 concentrating mechanism in several cyanobacterial strains: A review of general physiological characteristics, genes, proteins, and recent advances. *Can J Bot* 76:973–1002.
10. Badger MR, Price GD (2003) CO_2 concentrating mechanisms in cyanobacteria: Molecular components, their diversity and evolution. *J Exp Bot* 54:609–622.
11. Kaplan A (2017) On the cradle of CCM research: Discovery, development, and challenges ahead. *J Exp Bot* 68:3785–3796.
12. Figge RM, Cassier-Chauvat C, Chauvat F, Cerff R (2001) Characterization and analysis of an NAD(P)H dehydrogenase transcriptional regulator critical for the survival of cyanobacteria facing inorganic carbon starvation and osmotic stress. *Mol Microbiol* 39:455–468.
13. Wang HL, Postier BL, Burnap RL (2004) Alterations in global patterns of gene expression in *Synechocystis* sp. PCC 6803 in response to inorganic carbon limitation and the inactivation of ndhR, a LysR family regulator. *J Biol Chem* 279:5739–5751.
14. Woodger FJ, Bryant DA, Price GD (2007) Transcriptional regulation of the CO_2-concentrating mechanism in a euryhaline, coastal marine cyanobacterium, *Synechococcus* sp. strain PCC 7002: Role of NdhR/CcmR. *J Bacteriol* 189:3335–3347.
15. Burnap RL, Nambudiri R, Holland S (2013) Regulation of the carbon-concentrating mechanism in the cyanobacterium *Synechocystis* sp. PCC6803 in response to changing light intensity and inorganic carbon availability. *Photosynth Res* 118:115–124.
16. Omata T, Gohta S, Takahashi Y, Harano Y, Maeda S (2001) Involvement of a CbbR homolog in low CO_2-induced activation of the bicarbonate transporter operon in cyanobacteria. *J Bacteriol* 183:1891–1898.
17. Nishimura T, et al. (2008) Mechanism of low CO_2-induced activation of the cmp bicarbonate transporter operon by a LysR family protein in the cyanobacterium *Synechococcus elongatus* strain PCC 7942. *Mol Microbiol* 68:98–109.
18. Klähn S, et al. (2015) Integrated transcriptomic and metabolomic characterization of the low-carbon response using an *ndhR* mutant of *Synechocystis* sp. PCC 6803. *Plant Physiol* 169:1540–1556.
19. Daley SM, Kappell AD, Carrick MJ, Burnap RL (2012) Regulation of the cyanobacterial CO2-concentrating mechanism involves internal sensing of NADP+ and α-ketogutarate levels by transcription factor CcmR. *PLoS One* 7:e41286.
20. Kent SS, Young JD (1980) Simultaneous kinetic analysis of ribulose 1,5-bisphosphate carboxylase/oxygenase activities. *Plant Physiol* 65:465–468.
21. Hagemann M, et al. (2013) Evolution of the biochemistry of the photorespiratory C2 cycle. *Plant Biol (Stuttg)* 15:639–647.
22. Schell MA (1993) Molecular biology of the LysR family of transcriptional regulators. *Annu Rev Microbiol* 47:597–626.
23. Haimovich-Dayan M, Lieman-Hurwitz J, Orf I, Hagemann M, Kaplan A (2015) Does 2-phosphoglycolate serve as an internal signal molecule of inorganic carbon deprivation in the cyanobacterium *Synechocystis* sp. PCC 6803? *Environ Microbiol* 17: 1794–1804.
24. Schwarz D, Orf I, Kopka J, Hagemann M (2014) Effects of inorganic carbon limitation on the metabolome of the *Synechocystis* sp. PCC 6803 mutant defective in *glnB* encoding the central regulator PII of cyanobacterial C/N acclimation. *Metabolites* 4: 232–247.
25. Saint-Girons I, et al. (1986) Interactions of the *Escherichia coli* methionine repressor with the *metF* operator and with its corepressor, S-adenosylmethionine. *J Biol Chem* 261:10936–10940.
26. Arvidson DN, Bruce C, Gunsalus RP (1986) Interaction of the *Escherichia coli trp* aporepressor with its ligand, L-tryptophan. *J Biol Chem* 261:238–243.
27. Gajiwala KS, Burley SK (2000) Winged helix proteins. *Curr Opin Struct Biol* 10:110–116.
28. Zhou X, et al. (2010) Crystal structure of ArgP from Mycobacterium tuberculosis confirms two distinct conformations of full-length LysR transcriptional regulators and reveals its function in DNA binding and transcriptional regulation. *J Mol Biol* 396: 1012–1024.
29. Muraoka S, et al. (2003) Crystal structure of a full-length LysR-type transcriptional regulator, CbnR: Unusual combination of two subunit forms and molecular bases for causing and changing DNA bend. *J Mol Biol* 328:555–566.
30. Sainsbury S, et al. (2009) The structure of CrgA from Neisseria meningitidis reveals a new octameric assembly state for LysR transcriptional regulators. *Nucleic Acids Res* 37: 4545–4558.
31. Monferrer D, et al. (2010) Structural studies on the full-length LysR-type regulator TsaR from Comamonas testosteroni T-2 reveal a novel open conformation of the tetrameric LTTR fold. *Mol Microbiol* 75:1199–1214.
32. Ruangprasert A, Craven SH, Neidle EL, Momany C (2010) Full-length structures of BenM and two variants reveal different oligomerization schemes for LysR-type transcriptional regulators. *J Mol Biol* 404:568–586.
33. Taylor JL, et al. (2012) The crystal structure of AphB, a virulence gene activator from Vibrio cholerae, reveals residues that influence its response to oxygen and pH. *Mol Microbiol* 83:457–470.
34. Jo I, et al. (2015) Structural details of the OxyR peroxide-sensing mechanism. *Proc Natl Acad Sci USA* 112:6443–6448.
35. Lerche M, et al. (2016) The solution configurations of inactive and activated DntR have implications for the sliding dimer mechanism of LysR transcription factors. *Sci Rep* 6:19988.
36. Maddocks SE, Oyston PCF (2008) Structure and function of the LysR-type transcriptional regulator (LTTR) family proteins. *Microbiology* 154:3609–3623.
37. Yan D, Lenz P, Hwa T (2011) Overcoming fluctuation and leakage problems in the quantification of intracellular 2-oxoglutarate levels in *Escherichia coli*. *Appl Environ Microbiol* 77:6763–6771.
38. Muro-Pastor MI, Reyes JC, Florencio FJ (2001) Cyanobacteria perceive nitrogen status by sensing intracellular 2-oxoglutarate levels. *J Biol Chem* 276:38320–38328.
39. Zhang S, Bryant DA (2011) The tricarboxylic acid cycle in cyanobacteria. *Science* 334: 1551–1553.
40. Doucette CD, Schwab DJ, Wingreen NS, Rabinowitz JD (2011) α-Ketoglutarate coordinates carbon and nitrogen utilization via enzyme I inhibition. *Nat Chem Biol* 7: 894–901.
41. Henikoff S, Haughn GW, Calvo JM, Wallace JC (1988) A large family of bacterial activator proteins. *Proc Natl Acad Sci USA* 85:6602–6606.
42. Mittal M, Singh AK, Kumaran S (2017) Structural and biochemical characterization of ligand recognition by CysB, the master regulator of sulfate metabolism. *Biochimie* 142:112–124.
43. Espinosa J, Forchhammer K, Burillo S, Contreras A (2006) Interaction network in cyanobacterial nitrogen regulation: PipX, a protein that interacts in a 2-oxoglutarate dependent manner with PII and NtcA. *Mol Microbiol* 61:457–469.
44. Pflüger-Grau K, Görke B (2010) Regulatory roles of the bacterial nitrogen-related phosphotransferase system. *Trends Microbiol* 18:205–214.
45. Lieman-Hurwitz J, et al. (2009) A cyanobacterial AbrB-like protein affects the apparent photosynthetic affinity for CO_2 by modulating low-CO_2-induced gene expression. *Environ Microbiol* 11:927–936.
46. Kupriyanova EV, et al. (2013) CO_2-concentrating mechanism in cyanobacterial photosynthesis: Organization, physiological role, and evolutionary origin. *Photosynth Res* 117:133–146.
47. Hisbergues M, Jeanjean R, Joset F, Tandeau de Marsac N, Bédu S (1999) Protein PII regulates both inorganic carbon and nitrate uptake and is modified by a redox signal in *synechocystis* PCC 6803. *FEBS Lett* 463:216–220.
48. Lee HM, Vázquez-Bermúdez MF, de Marsac NT (1999) The global nitrogen regulator NtcA regulates transcription of the signal transducer PII (GlnB) and influences its phosphorylation level in response to nitrogen and carbon supplies in the Cyanobacterium *synechococcus* sp. strain PCC 7942. *J Bacteriol* 181:2697–2702.

Supporting Information

Jiang et al. 10.1073/pnas.1716062115

SI Materials and Methods

Expression and Purification of Recombinant NdhR. The coding region of the *ndhR* gene from *Synechocystis* was cloned into a pET28a-derived vector, which was further transformed into an *E. coli* strain harboring the pKY206 plasmid (BL21/pKY206) growing at 37 °C in LB culture medium (10 g NaCl, 10 g Bacto Tryptone (BD), and 5 g yeast extract/L). When the OD_{600} reached 0.8, expression of NdhR was induced for another 20 h at 16 °C by adding 0.2 mM isopropyl-β-D-thiogalactopyranoside. Cells were harvested and resuspended in 40 mL lysis buffer [20 mM Tris-Cl (pH 7.5), 1 M NaCl]. After sonication and centrifugation, the supernatant was loaded onto a nickel-nitrilotriacetic acid column preequilibrated with the lysis buffer. The target protein was eluted with 500 mM imidazole and further loaded onto a HiLoad 16/60 Superdex 200 column (GE Healthcare). Fractions containing the target protein were concentrated to 10 mg/mL for crystallization. The expression of selenomethionine (SeMet)-substituted NdhR was performed in SeMet medium (M9 medium with 50 mg/L SeMet and the other essential amino acids at 50 mg/L). The RD domain of NdhR was expressed in *E. coli* strain BL21 (DE3) and was purified in a way similar to the full-length protein.

Crystallization, Data Collection, and Processing. Crystallization of the full-length NdhR was performed using a Mosquito robot (TTP Labtech) in 96-well plates (Greiner) at 16 °C. All crystals were grown using the hanging-drop vapor-diffusion method. Crystals were obtained from 0.2 M sodium citrate tribasic dihydrate, 0.1 M Hepes (pH 7.5), 20% (vol/vol) isopropanol for native and SeMet-substituted NdhR and 0.2 M $MgCl_2$, 0.1 M Hepes (pH 7.5), 30% (vol/vol) polyethylene glycol 400 for RD cocrystallized with 5 mM 2-PG. All crystals were transferred to the cryoprotectant [reservoir solution supplemented with 30% (vol/vol) glycerol] and flash-frozen with liquid nitrogen. The diffraction data were collected at 100 K in a liquid nitrogen stream using beamline 17U with a Q315r CCD (ADSC; MarResearch) at the Shanghai Synchrotron Radiation Facility. All diffraction data were indexed, integrated, and scaled with HKL2000 (1).

Structure Determination and Refinement. The structure of the full-length NdhR in complex with 2-OG was determined using the single-wavelength anomalous dispersion (SAD) phasing method (2). The SHELXD program (3) was used to locate the heavy atoms, and the phase was calculated by OASIS (4) and further improved with RESOLVE and Buccaneer (5). Automatic model building was carried out using AutoBuild in PHENIX (6). Afterward, the initial model was subjected to molecular replacement against the 2.60-Å native data of NdhR using MOLREP (7). The structure of the RD domain with 2-PG was determined by molecular replacement using the RD from the full-length NdhR structure as a search model. All structures were refined with REFMAC5 (8) in CCP4i (9) and Phenix.refine in PHENIX and then were rebuilt interactively using COOT (10). The final models were evaluated with MolProbity (11) and PROCHECK (12). The data collection and structure refinement parameters are listed in Table S1. All structure figures were prepared with PyMOL (https://pymol.org/2/).

SPR Assays. SPR experiments were performed at 25 °C using a Biacore 3000 instrument using HBS [20 mM Hepes (pH 7.5), 200 mM NaCl] and a flow rate of 30 μL/min. NdhR was covalently immobilized on the carboxymethyl dextran surface of the CM5 chip. The effector 2-PG or 2-OG was incubated for 1 min before injection into the flowcells for 5 min. All analyses were performed with BIAevaluation software. The equilibrium responses were plotted and fitted to a 1:1 Langmuir binding model using Origin 8.0 software (OriginLab Corp.).

To detect the binding affinity of NdhR toward its promoter region, a 140-bp biotinylated DNA fragment was cloned from the promoter region of *ndhR* using a 5′-biotinylated antisense primer. Biotinylated DNA fragments were dissolved in immobilization buffer [20 mM Hepes (pH 7.5), 200 mM NaCl, 5% glycerol] and injected onto the NeutrAvidin surface. NdhR was incubated with either 2-OG or 2-PG for 5 min at a final concentration of 5 mM.

Mutant Construction. The *ndhR* deletion (Δ*ndhR*) in *Synechocystis* was constructed by replacing the *ndhR* gene with the cassette encoding a spectinomycin resistance gene via homologous recombination. The upstream and downstream sequences of *ndhR* were amplified by PCR and were further fused with the spectinomycin cassette gene. This fragment was cloned into the pUC19 plasmid, which was mixed with *Synechocystis* for homologous recombination. The cells were cultured at 30 °C with continuous illumination of 20 μmol photons·m^{-2}·s^{-1} for 4–6 h. The deletion of *ndhR* in *Synechocystis* was validated by PCR.

The POE strain was constructed by overexpressing the *slr0458* gene in *Synechocystis*. The *slr0458* gene was fused with the *slr0009* (*rbcL*) promoter and the ribosome-binding site (RBS) with the sequence of 5′-ACTAGAGTAGTGGAGGTTACTAG-3′, as well as the BBa-B0015 terminator (13), which was then cloned into a cargo plasmid, pRL1272, via homologous recombination. Then the conjugation reaction was performed in the *E. coli* Alice strain bearing the helper plasmid pRL623 and the conjugative plasmid pRL443. When OD600 reached 0.6 ∼ 0.8, the Alice strain was mixed with the wild-type or Δ*ndhR* strain of *Synechocystis* and incubated at 30 °C for 4–6 h.

RNA Extraction and Real-Time qRT-PCR. The *Synechocystis* cells were harvested from 10-mL cultures by centrifugation (12,000 × *g* for 5 min) and then were washed twice with the PBS buffer. RNA was extracted using the Eastep Super Total RNA Extraction Kit (Promega) according to the provided protocol. The RNA pellets were eluted and dissolved in 60–80 μL DNase/RNase/protease-free water and stored at −80 °C. The residual DNA was removed by RNase-free DNase (Takara) at 37 °C for 1–2 h.

cDNA synthesis was carried out using the PrimeScript RT Reagent Kit (Takara). For real-time PCR, amplifications were performed in a total volume of 20 μL using the FastStart Universal SYBR Green Master (Roche). The *rnpB* gene was used as a reference, and the target genes *slr0458*, *ndhR*, *ndhF3*, *sbtA*, and *bicA* were compared using the $2^{-\Delta\Delta}$ Ct method. The sequences of the primers used for the qRT-PCR analysis are listed in Table S2.

1. Otwinowski Z, Minor W (1997) Processing of X-ray diffraction data collected in oscillation mode. *Methods Enzymol* 276:307–326.
2. Brodersen DE, et al. (2000) Applications of single-wavelength anomalous dispersion at high and atomic resolution. *Acta Crystallogr D Biol Crystallogr* 56:431–441.
3. Sheldrick GM (2008) A short history of SHELX. *Acta Crystallogr A* 64:112–122.
4. Hao Q, Gu YX, Zheng CD, Fan HF (2000) OASIS: A computer program for breaking phase ambiguity in one-wavelength anomalous scattering or single isomorphous substitution (replacement) data. *J Appl Crystallogr* 33:980–981.
5. Cowtan K (2006) The Buccaneer software for automated model building. 1. Tracing protein chains. *Acta Crystallogr D Biol Crystallogr* 62:1002–1011.

6. Adams PD, et al. (2010) PHENIX: A comprehensive Python-based system for macromolecular structure solution. *Acta Crystallogr D Biol Crystallogr* 66:213–221.
7. Read RJ (2001) Pushing the boundaries of molecular replacement with maximum likelihood. *Acta Crystallogr D Biol Crystallogr* 57:1373–1382.
8. Murshudov GN, Vagin AA, Dodson EJ (1997) Refinement of macromolecular structures by the maximum-likelihood method. *Acta Crystallogr D Biol Crystallogr* 53: 240–255.
9. Collaborative Computational Project, Number 4 (1994) The CCP4 suite: Programs for protein crystallography. *Acta Crystallogr D Biol Crystallogr* 50:760–763.
10. Emsley P, Cowtan K (2004) Coot: Model-building tools for molecular graphics. *Acta Crystallogr D Biol Crystallogr* 60:2126–2132.
11. Chen VB, et al. (2010) MolProbity: All-atom structure validation for macromolecular crystallography. *Acta Crystallogr D Biol Crystallogr* 66:12–21.
12. Laskowski RA, Macarthur MW, Moss DS, Thornton JM (1993) Procheck–A program to check the stereochemical quality of protein structures. *J Appl Crystallogr* 26:283–291.
13. Englund E, Liang F, Lindberg P (2016) Evaluation of promoters and ribosome binding sites for biotechnological applications in the unicellular cyanobacterium Synechocystis sp. PCC 6803. *Sci Rep* 6:36640.

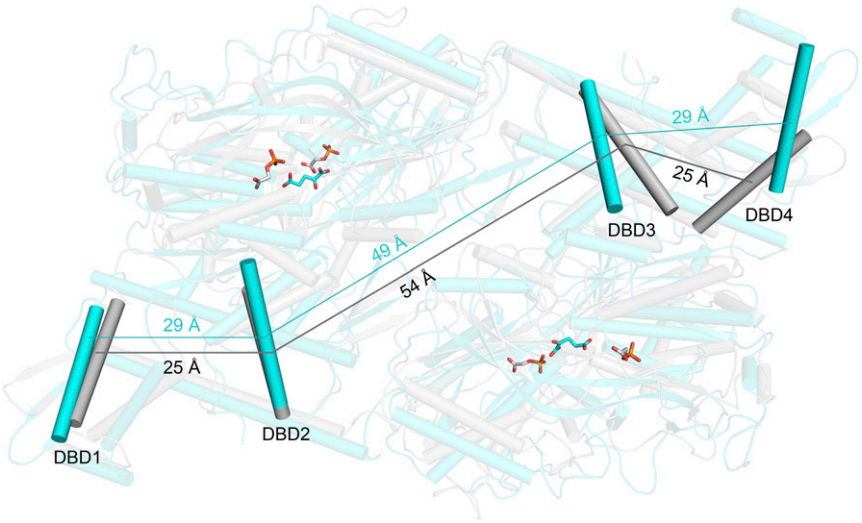

Fig. S1. A simulated model of full-length NdhR bound to 2-PG. Compared with the full-length structure of NdhR complexed with 2-OG (cyan), the binding of 2-PG showed drastic conformational changes of the NdhR tetramer (gray), as revealed by the 10-ns molecular dynamics simulations. Four DNA-recognition helices are shown as columns with distances between neighboring recognition helices labeled sequentially.

Table S1. Crystal parameters, data collection, and structure refinement

	SeMetNdhR+2-OG	NdhR+2-OG	NdhR-RD+2-PG
Data collection			
Space group	$P2_12_12_1$	$P2_12_12_1$	$P3_121$
Unit cell, Å (a,b,c)	93.15, 108.95, 179.27	90.77, 109.16, 178.23	58.97, 58.97, 123.96
Unit cell, ° (α,β,γ)	90.00	90.00	90.00, 90.00, 120.00
Resolution range, Å	65.85–2.75 (2.90–2.75)*	50.00–2.60 (2.63–2.60)	50.00–2.20 (2.28–2.20)
Unique reflections	48,102 (6,903)	52,491 (2,646)	13,083 (1,289)
Completeness, %	99.8 (99.9)	95.3 (97.5)	98.7 (99.1)
$<I/\sigma(I)>$	12.2 (3.4)	36.1 (3.3)	11.4 (3.3)
R_{merge} †,%	13.1 (73.7)	7.2 (51.3)	9.5 (50.1)
Average redundancy	11.4 (11.3)	4.8 (4.7)	4.8 (5.0)
Structure refinement			
Resolution range, Å		37.58–2.60	47.26–2.20
R-factor‡/R-free§, %		19.7/23.4	20.1/25.5
Number of protein atoms		9,634	1,661
Number of water atoms		111	39
Rmsd¶ bond lengths, Å		0.016	0.015
Rmsd bond angles, °		1.758	1.743
Mean B factors, Å^2		79.3	52.8
Ramachandran plot# residues, %			
Most favored, %		96.1	97.1
Additional allowed, %		3.9	2.9
Protein Data Bank ID code		5Y2V	5Y2W

*The values in parentheses refer to statistics in the highest bin.
†$R_{merge} = \sum_{hkl}\sum_i|I_i(hkl) - <I(hkl)>|/\sum_{hkl}\sum_i I_i(hkl)$, where $I_i(hkl)$ is the intensity of an observation, and $<I(hkl)>$ is the mean value for its unique reflection. Summations are over all reflections.
‡R-factor $= \sum_h|Fo(h) - Fc(h)|/\sum_h Fo(h)$, where Fo and Fc are the observed and calculated structure-factor amplitudes, respectively.
§R-free was calculated with 5% of the data excluded from the refinement.
¶Rmsd from ideal values.
#Categories were defined by MolProbity.

Table S2. qPCR primers used in this study

Primer	Forward (5′–3′)	Reverse (5′–3′)
rnpB	CTATGGCTCTAATCAATGGCACAC	CCTCAAGCGGTTCCACCAATCATG
slr0458	AGCAACGGGATTACCGCATTCT	ATGCCCACTTCTGCATCTTCTACG
ndhR	CCTTTAGTGGTCATTGCCCGTC	ACTACCCAATTCCAACCGCACC
ndhF3	ATGGCAATTCTGGTGATGTGTGTG	GGACGGTCATCGGCTTAGCTTCAC
sbtA	CCCGTGGCATTCTCTGTGATATTG	TGCTGAACGATTCCTCAATACTAG
bicA	GACCCGCACAGAACATAACTCC	AACTTTGAACGCAATACCAGCC